

Unambiguous detection of high energy vortex states via the superkick effect

Zhengjiang Li*

School of Physics and Astronomy, Sun Yat-sen University, Zhuhai 519082, China

Shiyu Liu* and Liangliang Ji†

*State Key Laboratory of High Field Laser Physics,
Shanghai Institute of Optics and Fine Mechanics (SIOM),
Chinese Academy of Sciences, Shanghai 201800, China*

Bei Liu* and Igor P. Ivanov‡

School of Physics and Astronomy, Sun Yat-sen University, Zhuhai 519082, China

(Dated: June 12, 2024)

Vortex states of photons, electrons, and other particles are freely propagating wave packets with helicoidal wave fronts winding around the axis of a phase vortex. A particle prepared in a vortex state possesses a non-zero orbital angular momentum projection on the propagation direction, a quantum number that has never been exploited in experimental particle and nuclear physics. Low-energy vortex photons, electrons, neutrons, and helium atoms have been demonstrated in experiment and found numerous applications, and there exist proposals of boosting them to higher energies. However, the verification that a high energy particle is indeed in a vortex state will be a major challenge, since the low energy techniques become impractical for highly energetic particles. Here, we propose a new diagnostic method based of the so-called superkick effect, which can unambiguously detect the presence of a phase vortex. A proof-of-principle experiment with vortex electrons can be done with the existing technology and will, at the same time, constitute the first observation of the superkick effect.

The structure and dynamics of composite systems, — atoms, nuclei, and hadrons, — is an immensely rich field of research. They are usually probed in collision-like experiments, be it atomic spectroscopy [1] or deep inelastic scattering of energetic electrons from protons [2]. Polarization of the initial particles provides access to additional information on the structure of the composite systems [3].

A decade ago it was realized that another, previously unexplored degree of freedom exists for particle collisions and has the potential to further expand the experimental capabilities in atomic, nuclear, and particle physics [4–7]. This new degree of freedom is the non-zero orbital angular momentum (OAM) projection on the propagation direction. Any particle, be it a photon, an electron, or a composite object such as a hadron, can be endowed with a well-controlled OAM by preparing it as a wave packet with helicoidal wave fronts, known as a vortex, or twisted, state. This wave packet possesses a phase singularity axis with zero intensity on the axis and the phase factor $\psi(\mathbf{r}) \propto e^{i\ell\varphi_r}$ in its vicinity, where φ_r is the azimuthal angle in the transverse plane. For a scalar particle, the factor $e^{i\ell\varphi_r}$ with the winding number ℓ implies a well-defined OAM $L_z = \hbar\ell$. For fermions and vector particles, the solutions must incorporate the spin-orbital interaction and can be constructed as eigenstates of the energy, helicity, and the total angular momentum projection J_z ; see the reviews [8–11] for the formalism.

Vortex photons are known in optics since decades [12] and have found numerous applications [13]. Vortex X rays have also been produced [14], and ideas on gener-

ating hard gamma photons in the MeV and GeV ranges have been outlined [5, 15, 16]. Following the proposal of [4], three groups produced in 2010–2011 vortex electrons with the kinetic energy 200–300 keV [17–19], which immediately found applications in nanoresearch [20]. Recently, cold neutrons [21] and slow helium atoms [22] were also put in vortex states. Various schemes of producing high energy vortex states of electrons and ions or of accelerating lower energy vortex particles to higher energies are being discussed, with first experimental proof-of-principle studies underway [23].

Once a vortex state is produced, one must verify that it indeed carries a non-zero OAM. A hallmark feature of a vortex state is its ring-shaped intensity profile in the transverse plane, which, for high-energy vortex electrons, can be revealed via inverse Compton scattering [24, 25], electron scattering on target atoms [26, 27], or Vavilov-Cherenkov radiation [28–30]. Although indicative of a vortex state, the ring-shaped intensity distribution alone cannot distinguish a phase vortex from a non-vortex ring-shaped wave function or an incoherent superposition of Gaussian wave packets. Vortex state can be unambiguously identified only if one directly probes the phase vortex and detects its winding number ℓ . At lower energies, this is routinely done, for example, with the aid of fork diffraction gratings [8–10]. For higher energy vortex states, this method becomes impractical due to the very short de Broglie wavelength and high penetrating power of high energy particles. Interference of the vortex state with a reference plane wave, another diagnostic tool used at lower energies, requires large transverse coher-

ence length, which may be unavailable in high energy vortex state generation. Finally, it was recently suggested that a generalized measurement procedure could be used in a generic scattering experiment to reveal the phase structure of the final particles wave function [31, 32]. However, this scheme relies on a completely new class of wavefront-sensitive detectors which are yet to be demonstrated at high energies.

In this Letter, we propose a method which can unmistakably reveal the presence of a phase vortex in a high-energy wave packet, which is free of the drawbacks of the previous suggestions. The method relies on elastic scattering of a vortex state with a compact non-vortex probe wave packet and reveals the existence of the phase vortex through the peculiar feature in the total final momentum angular distribution known as the superkick effect. The vortex beam is not blocked by any target, and the final state particles can be detected with traditional detectors. We will illustrate the idea with Møller (elastic e^-e^-) scattering, but the effect is purely kinematical and can be exploited for other initial particles. Experimental verification of our proposal will also constitute the first demonstration of the superkick effect itself.

Møller scattering of wave packets.—We begin with the plane-wave (PW) Møller scattering, in which two initial electrons with the four-momenta $k_1^\mu = (E_1, \mathbf{k}_1)$, $k_2^\mu = (E_2, \mathbf{k}_2)$ scatter elastically into the two final electrons with the four-momenta $k_3^\mu = (E_3, \mathbf{k}_3)$, $k_4^\mu = (E_4, \mathbf{k}_4)$. Throughout the paper, we use the relativistic Lorentz-Heaviside units $\hbar = c = 1$, $e^2 = 4\pi\alpha_{em}$, and denote three-vectors with bold symbols, adding the subscript \perp for transverse vectors. When giving the absolute values of the vectors, the bold symbols are dropped. We will also use the shorthand notation for the Lorentz-invariant momentum space measure

$$\widetilde{dk} \equiv \frac{d^3k}{2E(k)(2\pi)^3}. \quad (1)$$

The PW S -matrix element is

$$S_{PW} = i(2\pi)^4 \delta^{(4)}(k_1 + k_2 - k_3 - k_4) \frac{\mathcal{M} \cdot N_{PW}^4}{\sqrt{16E_1 E_2 E_3 E_4}}, \quad (2)$$

where $E(k) = \sqrt{k^2 + m_e^2}$, m_e being the electron mass. The invariant amplitude \mathcal{M} is calculated according to the Feynman rules [33]; its exact expression for general kinematics can be found in [34] and is reproduced in the Supplemental information. The factor $N_{PW} = 1/\sqrt{V}$ corresponds to the normalization of one particle per large volume V . Squaring S_{PW} and regularizing the delta-functions in the standard way [33], we obtain the differential cross section. Since the initial \mathbf{k}_1 and \mathbf{k}_2 are fixed, the total final state momentum $\mathbf{k}_3 + \mathbf{k}_4 \equiv \mathbf{K} = \mathbf{k}_1 + \mathbf{k}_2$ is also fixed.

Going beyond PW collisions, one can represent the initial particles as momentum space wave packets $\phi_1(\mathbf{k}_1)$

and $\phi_2(\mathbf{k}_2)$ normalized as $\int \widetilde{dk} |\phi_i(\mathbf{k})|^2 = 1$ and apply the scattering theory of arbitrarily shaped beams developed in [35–37]. A simplified version of this procedure was used in the first study of the so-called Bessel vortex particle scattering [5–7]. We focus on the head-on collision of wave packets which are centered around their respective average momenta $\mathbf{p}_1 = (p_1, 0, 0)$ and $\mathbf{p}_2 = (p_2, 0, 0)$, $p_2 < 0$. We also assume that the momentum spread inside each wave packet is much smaller than p_i , which allows us to treat the process in the paraxial approximation. With this notation, the differential probability of the wave packet scattering in an element of the final phase space can be written as

$$dW = (2\pi)^8 |\mathcal{I}|^2 \widetilde{dk}_3 \widetilde{dk}_4. \quad (3)$$

where

$$\mathcal{I} = \int \widetilde{dk}_1 \widetilde{dk}_2 \phi_1(\mathbf{k}_1) \phi_2(\mathbf{k}_2) \delta^{(4)}(k_1 + k_2 - K) \cdot \mathcal{M}. \quad (4)$$

Dividing the probability by an appropriately defined flux, one can obtain the generalized cross section [35, 37], see details in the Supplemental information. However, the key quantities are the probability and the eventual number of scattering events, not the cross section.

In Eq. (3), the two final particles are described as plane waves, and we introduced here their total momentum $K^\mu = (E_f, \mathbf{K})$. As the initial wave packets are no longer momentum eigenstates, the total final momentum \mathbf{K} is not fixed, and one can explore the differential cross section as a function not only of \mathbf{k}_3 but also of \mathbf{K} . In particular, if the two colliding wave packets, in coordinate space, have the transverse extents $\sigma_{1\perp}$ and $\sigma_{2\perp}$, the total final transverse momentum \mathbf{K}_\perp is expected to be distributed within the range of $\Sigma_K = 1/\sigma_{1\perp} + 1/\sigma_{2\perp}$. Note that the transverse momentum of each final electron, $|\mathbf{k}_3|$ and $|\mathbf{k}_4|$, can be much larger; it is their sum which is expected to be within this range.

The superkick effect.—Let us apply this scheme to the specific case of a vortex Laguerre-Gaussian (LG) wave packet colliding with a compact Gaussian wave packet, Fig. 1. In coordinate space, the two wave packets centroids follow parallel lines separated by a transverse impact parameter \mathbf{b}_\perp . We choose the LG wave packet in the principal radial mode described by the momentum space wave function

$$\phi_1(\mathbf{k}_1) \propto \frac{(\sigma_{1\perp} k_{1\perp})^\ell}{\sqrt{\ell!}} e^{i\ell\varphi_k} e^{-k_{1\perp}^2 \sigma_{1\perp}^2 / 2} e^{-(k_{1z} - p_1)^2 \sigma_{1z}^2 / 2}$$

and the Gaussian wave packet

$$\phi_2(\mathbf{k}_2) \propto e^{-i\mathbf{b}_\perp \cdot \mathbf{k}_{2\perp}} e^{-k_{2\perp}^2 \sigma_{2\perp}^2 / 2} e^{-(k_{2z} - p_2)^2 \sigma_{2z}^2 / 2}$$

for the counter propagating probe. The transverse $\sigma_{1\perp}$, $\sigma_{2\perp}$ and longitudinal σ_{1z} , σ_{2z} extents can be chosen independently, see the Supplemental material for more detail.

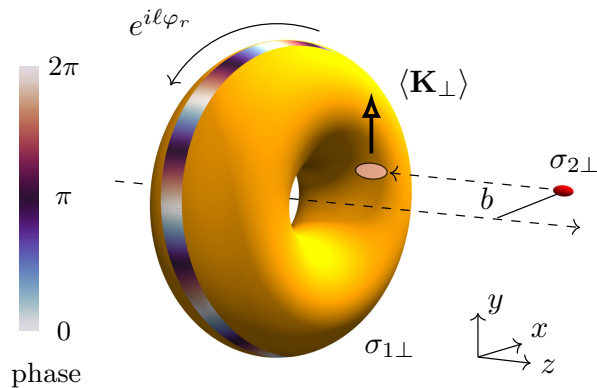


FIG. 1. A broad LG and a compact Gaussian wave packets of the transverse sizes of $\sigma_{1\perp}$ and $\sigma_{2\perp}$ collide at a non-zero impact parameter b along axis x . The donut shape with a colored stripe schematically shows the region of high intensity and the phase of the LG wave packet. In the overlap region, shown by the pink ellipse, the azimuthally varying phase induces an overall total transverse momentum $\langle \mathbf{K}_\perp \rangle$ orthogonal to \mathbf{b}_\perp .

The problem we consider possesses three transverse spatial scales: the widths of the two wave packets at maximal focusing $\sigma_{1\perp}$ and $\sigma_{2\perp}$ and the impact parameter $b \equiv |\mathbf{b}_\perp|$. We focus here on the regime when $\sigma_{1\perp} \gg \sigma_{2\perp}$ and $b \lesssim \sigma_{1\perp}$, that is, when a compact Gaussian wave packet scans the wider LG ring. In this setting, the average total transverse momentum of the two scattered electrons is $\langle \mathbf{K}_\perp \rangle \neq 0$. Moreover, it has a component orthogonal to \mathbf{b}_\perp . This is due to the asymmetric collision setting: the Gaussian wave packet is shifted from the vortex axis, experiences the phase factor $e^{i\ell\varphi_r}$, and, as a result, locally probes the azimuthal component of the LG state momentum distribution. What is surprising is that $\langle \mathbf{K}_\perp \rangle$ can be much larger than $\sqrt{\ell}/\sigma_{1\perp}$, the typical transverse momentum of the LG state. This unexpectedly large average total transverse momentum of the scattered final state, which emerged from the initial state with the zero average total transverse momentum, was dubbed in [38] as the superkick. Discussed in [38] in the context of twisted light absorbed by a trapped atom, the phenomenon was later predicted for hadronic photo-production [39, 40], and was investigated in [41, 42] for generic two particle scattering. It should be stressed that the superkick effect has not yet been observed experimentally, the main difficulty being the challenge of detecting the transverse momentum transfer to a trapped atom upon absorption of a vortex photon.

Semiclassically, the superkick effect originates from the rapidly varying phase factor near the phase singularity axis. As we go around the axis at a distance b , the phase factor $e^{i\ell\varphi_r}$ accumulates the phase change $2\pi\ell$ along the circle of circumference $2\pi b$. This rapid phase variation can be interpreted as the azimuthal component of the

local momentum distribution, $p_\varphi = \ell/b$. In the vicinity of the axis, $b \ll \sigma_{1\perp}$, this local momentum $p_\varphi \gg 1/\sigma_{1\perp}$ and becomes arbitrarily large as $b \rightarrow 0$. The compact Gaussian wave packet of the transverse extent $\sigma_{2\perp}$ allows us to probe this local transverse momentum down to $b \sim \sigma_{2\perp}$. Upon scattering, the total transverse momentum distribution is shifted away from zero to the direction orthogonal to the transverse impact parameter \mathbf{b}_\perp reaching the values up to $\ell/\sigma_{2\perp}$. The apparent paradox of the violation of the total transverse momentum conservation law is resolved in [41] by taking into account the non-scattered part of the colliding state wave functions.

The proposal.—The superkick effect is an unambiguous signature of a phase vortex. In order to prove that a high energy electron is in a vortex state, we propose to run an elastic scattering experiment at a fixed b . For each scattering event, both scattered electrons must be detected in coincidence and, from the measurement of their transverse momenta, one determines the total final momentum \mathbf{K} . Accumulating sufficient statistics, one obtains a distribution of the scattering events in the total transverse momentum \mathbf{K}_\perp . Repeating this experiment at several values of b , one effectively scans the LG state and tracks the change of the \mathbf{K}_\perp distribution as a function of b . In the absence of a phase vortex, we expect \mathbf{K}_\perp to be centered around zero or shifted along \mathbf{b}_\perp . The presence of the phase factor $e^{i\ell\varphi_r}$, which can only exist in the vicinity of a phase vortex, unavoidably shifts this distribution in the direction orthogonal to \mathbf{b}_\perp .

Numerical results.—To corroborate the above qualitative discussion, we undertook a numerical study of Møller scattering of an LG and a Gaussian wave packet using the exact expressions for the wave functions and for the scattering amplitudes, see the Supplemental material. Our benchmark case corresponds to the following parameters of the initial electrons: $p_{1z} = -p_{2z} = 10$ MeV, the total AM of the LG electron is $j_z = 7/2$, both electrons are unpolarized. The transverse wave packet sizes are $\sigma_{1\perp} = 10$ nm, $\sigma_{2\perp} = 2$ nm, so that $1/\sigma_{2\perp} = 100$ eV, $\sigma_{iz} = \sigma_{i\perp}/2$. The impact parameter is chosen along axis x : $\mathbf{b}_\perp = (b, 0)$, with values of b ranging from zero to 40 nm, well beyond the size of the LG ring.

Starting from Eq. (3), let us integrate over the longitudinal momenta of the two final electrons and, keeping \mathbf{K}_\perp fixed, over the transverse momentum of one of the electrons $\mathbf{k}_{3\perp}$ in the region $|\mathbf{k}_{3\perp}| > k_{3\min}$:

$$w_K = (2\pi)^2 \int \frac{d^3 k_3}{2E_3} \frac{dk_{4z}}{2E_4} |\mathcal{I}|^2. \quad (5)$$

The resulting quantity is the differential scattering probability, $w_K = dW/d^2 K_\perp$, and our task is to verify if it indeed displays a shift in the direction orthogonal to \mathbf{b}_\perp .

In Fig. 2(a)–(c), we show w_K for several values of $b = 1, 5, 15$ nm and for the cut-off value of $k_{3\min} = 1$ keV. In all cases, we observe a significant shift of the intensity

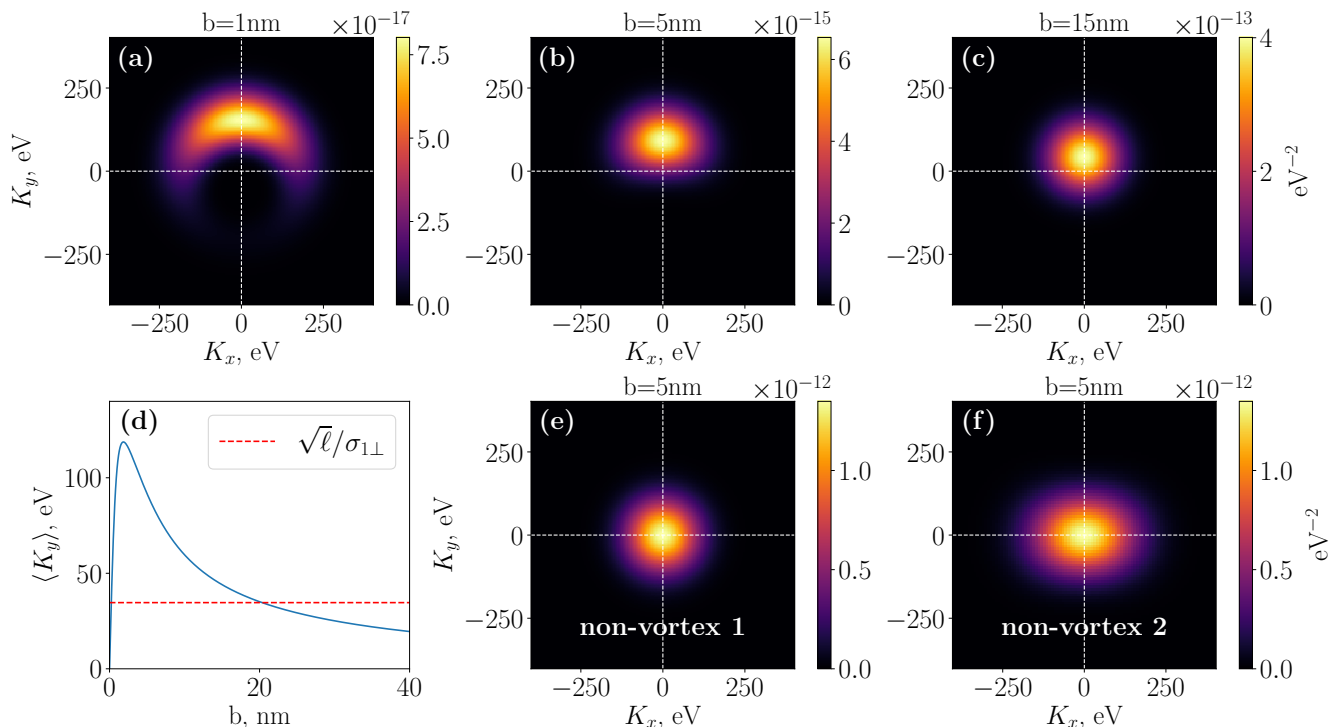


FIG. 2. Upper row, (a)–(c): differential scattering probability $w_K(\mathbf{K}_\perp)$ for $\mathbf{b}_\perp = (b, 0)$ with $b = 1, 5, 15$ nm. In all cases, $k_{min} = 1$ keV. Lower row, (d): the average value of $\langle K_y \rangle$ as a function of b . (e), (f): the differential probability $w_K(\mathbf{K}_\perp)$ for two examples of non-vortex wave packets (see main text).

peak towards positive K_y values, which is orthogonal to $\mathbf{b}_\perp = (b, 0)$. The evolution of the $\langle K_y \rangle$ as a function of b is shown in Fig. 2(d), and it follows the expected superkick dependence discussed in [38, 41, 42]. We also cross-checked these numerical results with analytical calculations. Namely, since $k_{3\perp} \gg K_\perp$, the invariant amplitude \mathcal{M} in Eq. (4) is nearly constant and can be taken out of the integral, dramatically simplifying the calculations in the spirit of Ref. [42].

To demonstrate that $\langle \mathbf{K}_\perp \rangle \perp \mathbf{b}_\perp$ is indeed an unmistakable feature of a phase vortex, we show in Fig. 2(e),(f) the same quantity w_K computed for two examples of non-vortex states which exhibit a ring intensity profile either in momentum space or in coordinate space: Fig. 2(e) corresponds to a state with the same $\phi_1(\mathbf{k}_1)$ as for the LG state but without the factor $e^{i\ell\varphi_k}$, while Fig. 2(f) has with same coordinate space wave function as the LG state but lacks the $e^{i\ell\varphi_r}$ factor. Both cases are calculated for the same Gaussian probe placed at $b = 5$ nm. We see that the non-vortex states never lead to the $\langle \mathbf{K} \rangle$ component orthogonal to \mathbf{b}_\perp .

Feasibility study.—The plots in Fig. 2, which show very different \mathbf{K}_\perp distributions for a vortex and non-vortex states, correspond to the ideal situation of unlimited statistics, absolutely stable beams, and perfect final electron momentum resolution. In a realistic experiment, these conditions will not be met, which requires

us to study how uncertainties and limited statistics affect the visibility of the effect.

We consider the transverse localization parameters $\sigma_{1\perp}$ and $\sigma_{2\perp}$ as realistic. In fact, much tighter focusing of vortex electrons has already been demonstrated in electron microscopes [20], with the focal spot of about 0.1 nm. However, bringing two wave packets in collision can lead to transverse jitter, event-by-event fluctuations of the impact parameter \mathbf{b}_\perp . We allow \mathbf{b}_\perp to fluctuate around $\langle \mathbf{b}_\perp \rangle = (\bar{b}, 0)$ in an azimuthally symmetric range with radius $|\Delta \mathbf{b}_\perp| = 2\sigma_{2\perp}$ (jitter as big as the Gaussian probe diameter). To account for it, we average w_K over the above range of \mathbf{b}_\perp and obtain the smeared differential probability $\bar{w}_K = \langle w_K \rangle_b$. The average value of \mathbf{K}_\perp is now computed based on the smeared probability \bar{w}_K . The effects of a possible longitudinal jitter are negligible due to the large Rayleigh length: $L = \sigma_{2\perp}^2 |p_{2z}| \sim 200 \mu\text{m}$ for our parameters.

To estimate the number of events expected in a realistic experiment, we integrate \bar{w}_K with respect to \mathbf{K}_\perp and obtain the total scattering probability $W(\bar{b})$. At $b \rightarrow 0$, the two wave packets miss each other, and the probability is extremely small. However, for $b \sim \sigma_{1\perp}$, it grows to $\mathcal{O}(10^{-8})$, see details in the Supplemental material. Multiplying by the total number N_0 of electron pair collisions, we expect to observe on average $N(\bar{b}) = N_0 W(\bar{b})$ scattering events. For definiteness, we consider electron

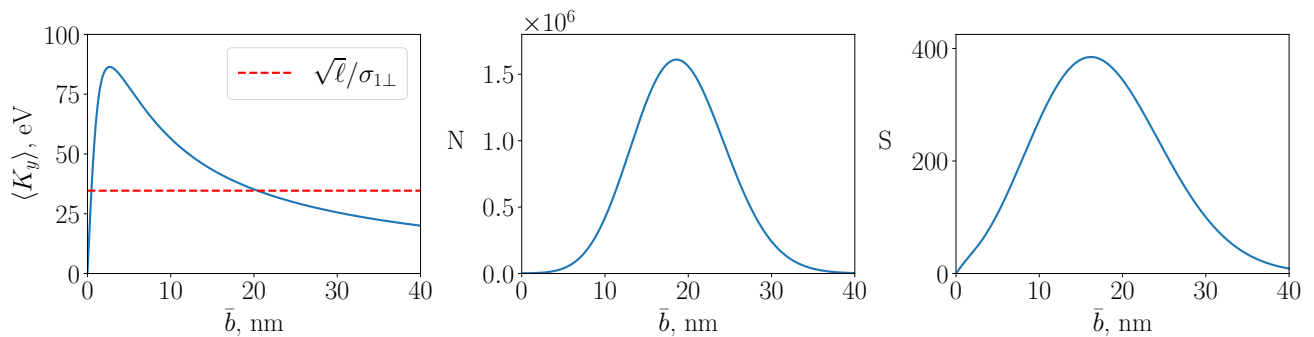


FIG. 3. The value of $\langle K_y \rangle$ (left), the number of events (middle), and the statistical significance of a non-zero $\langle K_y \rangle$ (right) as functions of the average impact parameter \bar{b} . Transverse jitter and a finite momentum resolution are taken into account.

beams at the average current of 16 nA, which corresponds to 10^{11} electrons per second. At this current, sequential electrons in each beam are separated by ~ 0.3 nm, which is sufficiently large to neglect the potentially detrimental space-charge effect on vortex electrons. An experiment running for 10^3 seconds yields $N_0 = 10^{14}$ electron collision attempts, and, for $b \sim \sigma_{1\perp}$, we expect to detect about million events. Thus, detection of the transverse shift in \bar{w}_K should be feasible.

Finally, we assume that the transverse momenta of the scattered electrons are measured with a finite uncertainty δk_\perp . To stay conservative, we take $\delta k_\perp = 1/\sigma_{2\perp}$, which means that the detector is unable to resolve the momentum-space ring structure of the LG wave packet and barely resolves the transverse momentum spread in the Gaussian probe.

Given all these imperfections and limited statistics, our goal is to detect with sufficient confidence that $\langle \mathbf{K}_y \rangle$ is indeed non-zero. The figure-of-merit is the statistical significance which we define as

$$S(\bar{b}) = \frac{\langle \mathbf{K}_y \rangle \sqrt{N(\bar{b})}}{\sqrt{\langle \mathbf{K}_y^2 \rangle + (\delta k_\perp)^2}}. \quad (6)$$

We consider the effect to be clearly visible if $S > 5$.

In Fig. 3, we show $\langle K_y \rangle$, the number of scattering events $N(\bar{b})$, and the statistical significance of the non-zero $\langle K_y \rangle$ as we scan \bar{b} across the vortex. By comparing Fig. 3, left, with Fig. 2(d), we observe the detrimental effect of the transverse jitter, which smears the observed distribution. As a result, although the superkick effect is expected to be the strongest at $b \ll \sigma_{1\perp}$, the very low scattering probability and jitter make the non-zero $\langle K_y \rangle$ poorly visible. However, for $b \sim \sigma_{1\perp}$, the statistical significance grows to value of a few hundred and makes the effect clearly visible. These figures demonstrated that the vortex-sensitive superkick effect will be observable even under larger jitter, poorer momentum resolution, and smaller statistics.

Conclusions.—In summary, collisions of high-energy vortex electrons, photons, and hadrons will offer a wealth

of information on the particle structure and dynamics, complementary to standard collision experiments. Realization of this research program will critically depend on unambiguous detection that a high-energy particle is indeed in a vortex state. The use of the existing low-energy diagnostic methods will be drastically limited in the MeV energy range and beyond, and other methods proposed in literature seem to imply serious challenges.

Here, we described a novel, superkick-based method to unmistakably detect the vortex state of a high-energy electron, which is free from the drawbacks of the other suggestions. We proposed to perform elastic scattering of a compact Gaussian probe electron with a vortex electron state at a controlled transverse impact parameter \mathbf{b}_\perp , detect the two scattered electrons using the traditional detectors, measure their total transverse momentum \mathbf{K}_\perp , and, with sufficient statistics, observe that the average value of $\langle \mathbf{K}_\perp \rangle$ has a sizable component orthogonal to \mathbf{b}_\perp . This feature can only be driven by the presence of a phase vortex and cannot be mimicked by non-vortex wave packets. Numerical calculations taking into account several possible experimental limitations confirm that the effect can be detected with very moderate requirements on the experimental setting.

A proof-of-principle experiment can be done with the existing moderately relativistic vortex electrons routinely produced in electron microscopes. One needs to arrange for collisions of vortex electrons with a counter-propagating tightly focused non-vortex electron beam, detect the scattered electrons in coincidence and measure their transverse momenta. There is no need to cover with the detectors the entire 2π range of the azimuthal angles; the expected statistical significance allows one to use compact detectors with limited angular angle coverage. Concrete predictions for a realistic experimental setting will be published elsewhere. Extension of this idea to detecting high-energy vortex photons, ions, and hadrons is straightforward and will also be elaborated in a future work.

ACKNOWLEDGMENTS

B.L. and I.P.I. are thankful to the Shanghai Institute of Optics and Fine Mechanics for hospitality during their visit. S.L. and L.J. thank the Sun Yat-sen University for hospitality during the workshop “Vortex states in nuclear and particle physics”, Zhuhai, April 2024. S.L. and L.J. acknowledge the support by National Science Foundation of China (Grant No. 12388102), CAS Project for Young Scientists in Basic Research (Grant No. YSBR060), and the National Key R&D Program of China (Grant No. 2022YFE0204800).

* These authors contributed equally to this work.

† jill@siom.ac.cn

‡ ivanov@mail.sysu.edu.cn

- [1] R. Kakkar, *Atomic and Molecular Spectroscopy: Basic Concepts and Applications* (Cambridge University Press, 2015).
- [2] R. G. Roberts, *The Structure of the proton: Deep inelastic scattering*, Cambridge Monographs on Mathematical Physics (Cambridge University Press, 1994).
- [3] C. A. Aidala, S. D. Bass, D. Hasch, and G. K. Mallot, *Rev. Mod. Phys.* **85**, 655 (2013), arXiv:1209.2803 [hep-ph].
- [4] K. Y. Bliokh, S. Savel'ev, and F. Nori, *Phys. Rev. Lett.* **99**, 190404 (2007), arXiv:0706.2486 [quant-ph].
- [5] U. D. Jentschura and V. G. Serbo, *Phys. Rev. Lett.* **106**, 013001 (2011), arXiv:1008.4788 [physics.acc-ph].
- [6] I. P. Ivanov, *Phys. Rev. D* **83**, 093001 (2011), arXiv:1101.5575 [hep-ph].
- [7] D. V. Karlovets, *Phys. Rev. A* **86**, 062102 (2012), arXiv:1206.6622 [hep-ph].
- [8] K. Y. Bliokh *et al.*, *Phys. Rept.* **690**, 1 (2017), arXiv:1703.06879 [quant-ph].
- [9] S. M. Lloyd, M. Babiker, G. Thirunavukkarasu, and J. Yuan, *Rev. Mod. Phys.* **89**, 035004 (2017).
- [10] B. A. Knyazev and V. G. Serbo, *Physics Uspekhi* **61**, 449 (2018).
- [11] I. P. Ivanov, *Prog. Part. Nucl. Phys.* **127**, 103987 (2022), arXiv:2205.00412 [hep-ph].
- [12] L. Allen, M. W. Beijersbergen, R. J. C. Spreeuw, and J. P. Woerdman, *Phys. Rev. A* **45**, 8185 (1992).
- [13] J. P. Torres and T. Lluis, *Twisted Photons: Applications of Light with Orbital Angular Momentum* (Wiley-VCH, 2011).
- [14] J. T. Lee, S. Alexander, S. Kevan, S. Roy, and B. McMorrnan, *Nature Photonics* **13**, 205 (2019).
- [15] Y. Taira, T. Hayakawa, and M. Katoh, *Sci. Rep.* **7**, 5018 (2017), arXiv:1608.04894 [physics.acc-ph].
- [16] Y.-Y. Chen, K. Z. Hatsagortsyan, and C. H. Keitel, *Matter and Radiation at Extremes* **4**, 024401 (2019).
- [17] M. Uchida and A. Tonomura, *Nature* **464**, 737 (2010).
- [18] J. Verbeeck, H. Tian, and P. Schattschneider, *Nature* **467**, 301 (2010).
- [19] B. J. McMorrnan, A. Agrawal, I. M. Anderson, A. A. Herzog, H. J. Lezec, J. J. McClelland, and J. Unguris, *Science* **331**, 192 (2011).
- [20] J. Verbeeck, P. Schattschneider, S. Lazar, M. Stöger-Pollach, S. Löffler, A. Steiger-Thirsfeld, and G. Van Tendeloo, *Applied Physics Letters* **99**, 203109 (2011).
- [21] D. Sarenac, M. E. Henderson, H. Ekinici, C. W. Clark, D. G. Cory, L. Debeer-Schmitt, M. G. Huber, C. Kapahi, and D. A. Pushin, *Science Advances* **8**, eadd2002 (2022).
- [22] A. Luski, Y. Segev, R. David, O. Bitton, H. Nadler, A. R. Barnea, A. Gorlach, O. Cheshnovsky, I. Kaminer, and E. Narevicius, *Science* **373**, 1105 (2021).
- [23] Workshop on “Vortex states in nuclear and particle physics”, Zhuhai, China, Apr 24–28, 2024, <https://indico.ihep.ac.cn/event/21491/> (2024).
- [24] D. Seipt, A. Surzhykov, and S. Fritzsche, *Phys. Rev. A* **90**, 012118 (2014), arXiv:1407.4329 [physics.optics].
- [25] Z. Bu, X. Geng, S. Liu, S. Lei, B. Shen, R. Li, Z. Xu, and L. Ji, (2023), arXiv:2302.05065 [physics.optics].
- [26] V. Serbo, I. P. Ivanov, S. Fritzsche, D. Seipt, and A. Surzhykov, *Phys. Rev. A* **92**, 012705 (2015), arXiv:1505.02587 [physics.atom-ph].
- [27] D. V. Karlovets, G. L. Kotkin, V. G. Serbo, and A. Surzhykov, *Phys. Rev. A* **95**, 032703 (2017), arXiv:1612.08252 [quant-ph].
- [28] I. Kaminer, M. Mutzafi, A. Levy, G. Harari, H. Herzog Sheinfux, S. Skirlo, J. Nemirovsky, J. D. Joannopoulos, M. Segev, and M. Soljačić, *Phys. Rev. X* **6**, 011006 (2016), arXiv:1411.0083 [quant-ph].
- [29] I. P. Ivanov, V. G. Serbo, and V. A. Zaytsev, *Phys. Rev. A* **93**, 053825 (2016), arXiv:1602.05099 [quant-ph].
- [30] A. D. Chaikovskaia, D. V. Karlovets, and V. G. Serbo, *Phys. Rev. A* **109**, 012222 (2024), arXiv:2310.09864 [quant-ph].
- [31] D. V. Karlovets, S. S. Baturin, G. Geloni, G. K. Sizykh, and V. G. Serbo, *Eur. Phys. J. C* **82**, 1008 (2022), arXiv:2201.07997 [hep-ph].
- [32] D. V. Karlovets, S. S. Baturin, G. Geloni, G. K. Sizykh, and V. G. Serbo, *Eur. Phys. J. C* **83**, 372 (2023), arXiv:2203.12012 [hep-ph].
- [33] V. B. Berestetskii, E. M. Lifshitz, and L. P. Pitaevskii, *Quantum Electrodynamics*, Course of Theoretical Physics, Vol. 4 (Pergamon Press, Oxford, 1982).
- [34] I. P. Ivanov, D. Seipt, A. Surzhykov, and S. Fritzsche, *Phys. Rev. D* **94**, 076001 (2016), arXiv:1608.06551 [hep-ph].
- [35] G. L. Kotkin, V. G. Serbo, and A. Schiller, *Int. J. Mod. Phys. A* **7**, 4707 (1992).
- [36] D. Karlovets, *Phys. Rev. A* **98**, 012137 (2018), arXiv:1803.10166 [quant-ph].
- [37] D. V. Karlovets and V. G. Serbo, *Phys. Rev. D* **101**, 076009 (2020), arXiv:2002.00101 [hep-ph].
- [38] S. M. Barnett and M. Berry, *Journal of Optics* **15**, 125701 (2013).
- [39] A. Afanasev, C. E. Carlson, and A. Mukherjee, *Phys. Rev. Res.* **3**, 023097 (2021), arXiv:2007.05816 [quant-ph].
- [40] A. Afanasev and C. E. Carlson, *Annalen Phys.* **534**, 2100228 (2022), arXiv:2105.07271 [hep-ph].
- [41] I. P. Ivanov, B. Liu, and P. Zhang, *Phys. Rev. A* **105**, 013522 (2022), arXiv:2109.01323 [quant-ph].
- [42] B. Liu and I. P. Ivanov, *Phys. Rev. A* **107**, 063110 (2023), arXiv:2212.03624 [hep-ph].
- [43] N. Sheremet, A. Chaikovskaia, D. Grosman, and D. Karlovets, (2024), arXiv:2404.11497 [physics.atom-ph].

SUPPLEMENTAL MATERIAL

Wave packets of initial electrons

Our calculations follow the scheme described in [42], which builds upon the general formalism of wave packet collisions [35, 37]. Let us begin with the scalar field wave packets. The initial particles are represented by momentum space wave packets $\phi_1(\mathbf{k}_1)$ and $\phi_2(\mathbf{k}_2)$ normalized as

$$\int \frac{d^3k}{(2\pi)^3} \frac{1}{2E(k)} |\phi_i(\mathbf{k})|^2 = 1. \quad (7)$$

$$\phi_1(\mathbf{k}_1) = (4\pi)^{3/4} \sigma_{1\perp} \sqrt{\sigma_{1z}} \sqrt{2E_1} \frac{(\sigma_{1\perp} k_{1\perp})^\ell}{\sqrt{\ell!}} \exp \left[-\frac{k_{1\perp}^2 \sigma_{1\perp}^2}{2} - \frac{(k_{1z} - p_{1z})^2 \sigma_{1z}^2}{2} + i\ell\varphi_k \right]. \quad (9)$$

Here, $\sigma_{1\perp}$ and σ_{1z} are the transverse and longitudinal spatial extents of the coordinate space wave function, which are considered independent parameters. We choose σ_{1z} to be of the same order as $\sigma_{1\perp}$ to guarantee that the wave packets do not significantly spread during the overlap time; this regime was called in [41] the impulse approximation. Using the LG modes with the radial quantum number $n > 0$ or the so-called elegant LG wave packets as, for example, in [43] is also possible not essential for presenting our main idea. The Gaussian state can be obtained from the above formula by setting $\ell = 0$:

$$\phi_2(\mathbf{k}_2) = (4\pi)^{3/4} \sigma_{2\perp} \sqrt{\sigma_{2z}} \sqrt{2E_2} \exp \left[-\frac{k_{2\perp}^2 \sigma_{2\perp}^2}{2} - \frac{(k_{2z} - p_{2z})^2 \sigma_{2z}^2}{2} - i\mathbf{b}_\perp \mathbf{k}_{2\perp} - ib_z k_{2z} + i\tau E_2 \right], \quad (10)$$

with parameters $\sigma_{2\perp}$ and σ_{2z} . Here, we also take into account the possibility that the two wave packets may be shifted with respect to each other in three different ways. The impact parameter \mathbf{b}_\perp defines the transverse offset between their axes, b_z defines the longitudinal distance between their focal planes, and τ characterizes the time difference between the instants of their maximal focusing. As described in [41, 42], b_z and τ play inessential role in the paraxial approximation due to the Rayleigh length (wave packet spreading distance) $L_R = \sigma_{2\perp}^2 |p_{2z}|$ being large even for the compact Gaussian beam. Thus, we can set b_z and τ to zero.

Next, taking into account that electrons have spin, we describe the internal degrees of freedom of the plane-wave electron with the four-momentum k^μ and helicity λ with the bispinor $u_{k\lambda}$:

$$u_{k\lambda} = \begin{pmatrix} \sqrt{E+m_e} w^{(\lambda)} \\ 2\lambda \sqrt{E-m_e} w^{(\lambda)} \end{pmatrix}. \quad (11)$$

Our choice of the spinors $w^{(\lambda)}$ is slightly different for the first and the second electron in Møller scattering. For the first electron in Møller scattering, the one with $k_{1z} > 0$,

The average momentum in each wave packets, $\mathbf{p}_1 = \langle \mathbf{k}_1 \rangle$ and $\mathbf{p}_2 = \langle \mathbf{k}_2 \rangle$, are antiparallel to each other and define the common axis z : $p_{1z} > 0$, $p_{2z} < 0$. We adopt the paraxial approximation, in which the typical transverse momenta are assumed to be much smaller than p_{1z} and $|p_{2z}|$. Strictly speaking, a localized wave packet is non-monochromatic, but in the paraxial approximation the energy distribution peaks around $\varepsilon_1 = \sqrt{p_1^2 + m^2}$ with an energy spread negligible for our purposes. The coordinate wave functions are defined by

$$\psi(\mathbf{r}, t) = \int \frac{d^3k}{(2\pi)^3} \frac{1}{\sqrt{2E(k)}} \phi(\mathbf{k}) e^{i\mathbf{k}\mathbf{r} - iE(\mathbf{k})t} \quad (8)$$

and are normalized as $\int d^3r |\psi(\mathbf{r}, t)|^2 = 1$.

For the scalar vortex state, we use the relativistic LG principal mode:

the spinors are

$$w^{(+1/2)} = \begin{pmatrix} c_1 \\ s_1 e^{i\varphi_1} \end{pmatrix}, \quad w^{(-1/2)} = \begin{pmatrix} -s_1 e^{-i\varphi_1} \\ c_1 \end{pmatrix}, \quad (12)$$

while the second, counter-propagating electron with $k_{2z} < 0$, is described with

$$w^{(+1/2)} = \begin{pmatrix} c_2 e^{-i\varphi_2} \\ s_2 \end{pmatrix}, \quad w^{(-1/2)} = \begin{pmatrix} -s_2 \\ c_2 e^{i\varphi_2} \end{pmatrix}. \quad (13)$$

Here, $c_i \equiv \cos(\theta_i/2)$, $s_i \equiv \sin(\theta_i/2)$, with θ_i and φ_i being the polar and azimuthal angles of \mathbf{k}_i . This choice possesses a well-define forward limit for the first electron $\theta_1 \rightarrow 0$, when $s_1 \rightarrow 0$, and a well-define backward limit for the second $\theta_2 \rightarrow \pi$, when $c_2 \rightarrow 0$. Similar conventions are used for the two final electrons in small-angle scattering. Note that, for non-zero θ_i , these bispinors are not eigenstates of the operators of the z -projections of spin or OAM. However, they are eigenstates of the z -projection of the total angular momentum operator $\hat{j}_z = \hat{s}_z + \hat{\ell}_z$ with the eigenvalues $j_z = \lambda_1$ for the first electron and $j_z = -\lambda_2$ for the second electron.

We define the initial electron wave packets in momentum space as $\phi_i(\mathbf{k}_i)u_{k_i\lambda_i}$. The resulting LG state of the first electron is not an eigenstate of the OAM or spin z -projections, but it is still an eigenstate of \hat{j}_z with the eigenvalue of $\ell + \lambda_1$, where ℓ is the parameter of the LG state in Eq. (9). Nevertheless, in the paraxial approximation, $\langle \hat{\ell}_z \rangle \approx \ell$, and although the OAM and the spin degrees of freedom are entangled due to the unavoidable spin-orbital interactions, one can conduct the calculations keeping in mind that the OAM and spin are approximately conserved.

Møller scattering of wave packets

In the main text, we defined the differential probability of the elastic scattering dW , which is the main observable in localized wave packet scattering. If needed, one can define the generalized cross section as $d\sigma = dW/L$, where the luminosity function, or the flux, for a general two wave packet collision can be found in [37]. Within the paraxial approximation, the relative velocity $|v_1 - v_2|$ can be computed via the average momenta of the two wave packets $v_i = p_{iz}/\varepsilon_i$ (with $v_1 > 0$ and $v_2 < 0$), which simplifies the expression and allows us to represent the luminosity function as a space-time overlap of the two colliding wave packets:

$$L = |v_1 - v_2| \int d^3r dt |\psi_1(\mathbf{r}, t)|^2 |\psi_2(\mathbf{r}, t)|^2. \quad (14)$$

This factor takes care of the correct normalization which is especially important when two the colliding wave packets overlap only partially. We stress once again that the primary observable is the scattering probability itself, which we analyze in the main text.

Next, the amplitude of the wave packet scattering into final plane waves is given by \mathcal{I} in Eq. (4) and is expressed via an appropriately weighted plane wave helicity amplitude \mathcal{M} . In the Born approximation, the plane-wave $ee \rightarrow e'e'$ helicity amplitude can be found, for example, in [33] and is given by

$$\mathcal{M} = e^2 \left(\frac{\bar{u}_3 \gamma^\mu u_1 \bar{u}_4 \gamma_\mu u_2}{t} - \frac{\bar{u}_4 \gamma^\mu u_1 \bar{u}_3 \gamma_\mu u_2}{u} \right). \quad (15)$$

Since we consider small-angle scattering, the Mandelstam invariants $|t| \ll |u|$, so that the t -channel amplitude dominates. The exact expressions for the helicity amplitudes $\lambda_1 \lambda_2 \rightarrow \lambda_3 \lambda_4$ in the generic kinematics were given in [34] and are used in our numerical calculations. In the ultrarelativistic, small scattering angle limit, each electron conserves its helicity and the expressions simplify to

$$\mathcal{M} \approx 8\sqrt{E_1 E_2 E_3 E_4} \frac{e^2}{t} \delta_{\lambda_1, \lambda_3} \delta_{\lambda_2, \lambda_4}. \quad (16)$$

Although this expression does not depend on whether $\lambda_1 = \lambda_3 = +1/2$ or $-1/2$, some care must be taken when

defining the unpolarized cross section. In this work we follow the prescription of [26, 34] to define the unpolarized vortex state as an equal mixture of positive and negative helicity states with the same value of the conserved quantity j_z , that is, the LG states with $\ell = j_z - 1/2$, $\lambda_1 = +1/2$ and $\ell = j_z + 1/2$, $\lambda_1 = -1/2$. The matter-of-principle conclusions of our paper remain the same even if an alternative definition of the unpolarized LG electron based on the same value of the parameter ℓ is used.

Estimating the scattering probability

The visibility of the effect depends on the expected number of scattering events. In the main text, in Fig. 2, we showed results of our numerical code. Here, we show how an order of magnitude estimate of the total number of events can be derived analytically.

As demonstrated in [42], the exact expression for \mathcal{I} in the superkick-related kinematics can be treated analytically in the paraxial and impulse approximation, that is, when the wave packets do not spread significantly during the collision event. Moreover, if the plane-wave scattering amplitude \mathcal{M} does not vary significantly inside the integral in Eq. (4), it can be taken out of the integral, simplifying the results. In our case, the main dependence of \mathcal{M} on \mathbf{k}_1 comes from $t \approx -(\mathbf{k}_{3\perp} - \mathbf{k}_{1\perp})^2$. Thus, as long as $|k_{3\perp}|_{\min} \gg 1/\sigma_{1\perp}$, we can approximate t with $-\mathbf{k}_{3\perp}^2$, take \mathcal{M} out of the integral, and get a close analytical estimate of the scattering probability W as a function of b and $k_{3\min}$.

There exists a shorter way to get this probability. As shown in [37] and explicitly verified in the superkick-related situation in [42], the integrated cross section of wave packet scattering well above the threshold is very close to the plane wave cross section σ_{PW} . The novel effects of the vortex state collisions appear primarily in the differential cross sections, not in the total ones. The interaction probability can be well approximated by $W = \sigma_{PW} \cdot L$, with the luminosity function given in Eq. (14). The elastic scattering cross section integrated over $|k_{3\perp}| > k_{3\min}$ is

$$\sigma_{PW} = \frac{4\pi\alpha_{em}^2}{k_{3\min}^2} \approx \frac{2 \times 10^{-5} \text{ nm}^2}{(k_{3\min} [\text{keV}])^2}. \quad (17)$$

The analytical expression for L was derived in [42] and, for $\sigma_{2\perp} \ll \sigma_{1\perp}$, it can be approximated by

$$L \approx \frac{1}{\pi \ell! \sigma_{1\perp}^2} \left(\frac{b^2}{\sigma_{1\perp}^2} \right)^\ell e^{-b^2/\sigma_{1\perp}^2}. \quad (18)$$

This expression is maximal at $b = \sqrt{\ell} \sigma_{1\perp}$, and for moderately large ℓ it yields $L \sim 0.1/\sigma_{1\perp}^2$. As a result, the order of magnitude estimate of the maximal scattering

probability is

$$W \sim \frac{10^{-6}}{(k_{3\min}[\text{keV}] \cdot \sigma_{1\perp}[\text{nm}])^2}. \quad (19)$$

For $\sigma_{1\perp} = 10$ nm, it gives $W \sim 10^{-8}$ and, with a sufficient current and experiment running time, can lead to

many thousands of detected events. A stronger focusing of the LG wave packet would boost the probability but, at the same time, would require us to increase the lower limit $k_{3\min}$ in order to be able to safely distinguish scattered and non-scattered states. If $b \ll \sigma_{1\perp}$, the luminosity function decreases rapidly, and the number of events may drop below one.